University of BRISTOL

DEPARTMENT OF MECHANICAL ENGINEERING

The Optimisation of 3D Printed Components

Jonathan Shindler

Supervisor: Dr James Gopsill

Report Submitted for the Degree of Engineering June 2015

Acknowledgements

I acknowledge Dr James Gopsill, my supervisor, who assisted in the development of the optimisation strategy presented in this paper and for offering guidance on the writing of this paper. I also acknowledge the rest of the staff in the Language of Collaborative Manufacturing office for providing the 3D printer and filament for this research. I acknowledge Peter Whereat, the technician who assisted in setting up the three point bend test and the Instron machines in the lab. I acknowledge Dr Henry Thomas for creating and freely providing the open source program GPX, which was used as a file converter. I acknowledge Jos van der Geest for his MATLAB function *insertrows*.

DECLARATION

> *The accompanying research project report entitled: The Optimisation of 3D Printed Components is submitted in the third year of study towards an application for the degree of Master of Engineering in Mechanical Engineering at the University of Bristol. The report is based upon independent work by the candidate. All contributions from others have been acknowledged above. The supervisors are identified at the start of the report. The views expressed within the report are those of the author and not of the University of Bristol.*

I hereby declare that the above statements are true.

Signed (author)

……………………………………………………………………………………………..

Full Name

……………………………………………………………………………………………..

Date

……………………………………………………………………………………………..

Declaration of Copyright

Certification of ownership of the copyright in a dissertation presented as part of and in accordance with the requirements for the Final Degree of Master of Engineering at the University of Bristol, Faculty of Engineering.

I hereby assert that I own exclusive copyright in the item named below. I give permission to the University of Bristol Library to add this item to its stock and to make it available for consultation in the library, and for inter-library lending for use in another library. It may be copied in full or in part for any bone fide library or research worker on the understanding that users are made aware of their obligations under the copyright legislation, i.e. that no quotation and no information derived from it may be published without the author's prior consent.

Author	*Jonathan Shindler*
Title	*The Optimisation of 3D Printed Components*
Date of Submission	*22/06/15*

Signed (author)

…………………………………………………………………………………………..

Full Name

…………………………………………………………………………………………..

Date

…………………………………………………………………………………………..

Summary

3 Dimensional (3D) printed components are printed with non-solid internal structures, known as infill patterns. A common infill pattern is a regular hexagonal structure. The main aim of the research presented in this paper is to develop a strategy to optimise the infill pattern of 3D printed components based on their loading conditions. The strategy developed splits the 3D printed component up into a regular rectangular grid. The stress distribution across the component calculated by FEA (Finite Element Analysis) is used to add more material to the cells in the grid which have higher stress values. This results in an optimised infill pattern based on the components loading conditions. To evaluate the strategy developed, two optimised beams were created by the strategy and printed. These were tested against hexagonally-infilled beams in a three point bend test. The flexural strength was measured and the strength-to-weight and strength-to-print time metrics were calculated. The best-performing optimised beam scored 16.3 N/gram and 4.7 N/minute in the two metrics respectively. This represented a 55% and 27% increase respectively compared to the best-performing hexagonally-infilled beam which scored 10.5 N/gram and 3.7 N/minute in the two metrics respectively. The relevance of these results is that, due to the success of testing the optimised beams, an optimisation strategy like this one could be incorporated into an FEA package. This would help widen the use of 3D printing in industry as optimised 3D components are cheaper to print due to them being stronger per unit weight.

Contents

List of Figures

1   Introduction

Additive manufacturing refers to a group of processes in which material is deposited layer by layer to build up a 3 Dimensional (3D) component or model. This differs from conventional subtractive methods, such as milling and machining, which start with a solid billet and remove material to create a final component.

There exists a variety of additive manufacturing techniques, of which the most common include Fused Deposition Modelling (FDM), Powdered Laser Sintering (PLS) and Electron Beam Sintering (EBS). PLS and EBS involve using a laser and an electron beam respectively to fuse metal powder together in lots of horizontal layers, building the model up vertically, whilst FDM melts and deposits material layer by layer through a nozzle. This research focuses on the latter and the next section describes the FDM process, and in particular, the Makerbot Desktop 2, which is the 3D printer used for this research.

1.1   Fused Deposition Modelling

In FDM, a filament of 1.75 mm diameter is heated to 230 °C and is extruded layer by layer through a 0.4 mm diameter nozzle onto a bed. The layer height is the height of each individual horizontal layer and is typically set at 0.2 mm, but can be varied to improve the quality of the model. A height of 0.1 mm is selected for high resolution models and 0.4 mm for models with lower resolution.

Figure 1 shows a schematic of the FDM process. The filament is loaded on a spool (1) and pulled through into the printer head by a small servo-motor (2). A spring-loaded tensioning unit provides tension to the filament to allow the motor to pull the filament through into the heating element where it is melted. It is then deposited onto the printer bed by the nozzle (3). The printer bed moves in the Z (vertical) direction via a lead screw whilst the printer head moves in the X and Y directions via two toothed belts attached to stepper motors. Some printers also have heated beds which assist in material adhesion to the bed.
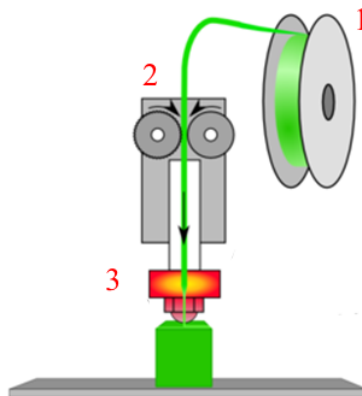
Figure 1: Schematic of FDM process. Reproduced from [1].

Thermoplastics are often the material of choice used for the FDM process; either Polylactic Acid (PLA) or Acrylonitrile Butadiene Styrene (ABS). The number of commercially available printable materials has been rapidly expanding for the FDM process, which include thermoplastics, nylon, brass, flexible plastic and dissolvable plastic.

FDM systems are more commonly known as 3D printers. Recent patent expirations in the field of 3D printing has lead to the widespread expansion of the 3D printer market. This expansion is due to the decrease in price of printers as a result of increased competition and

also due to open-source printers such as the Rep-Rap [4]. RepRaps are bare-bones 3D printers which are designed to be semi self-replicable and require assembly by the user. Canalys, an industry analyst, has predicted that the global market for 3D printers and 3D printing will grow from $2.5 billion in 2013 to $16.2 billion by 2018 [5]. Gartner, an American research and advisory firm has estimated that shipments of 3D printers around the world will reach around 217,350 units in 2015. This is a significant increase of just over double since 2014, when the estimated number of units shipped was 108,150 [6].

3D printers have become cheaper and more accessible to the general public and to the hobbyist due to the introduction of home 3D printers. Printers available include the Maker-bot Desktop 2 and a variety of RepRap models. However, the use of 3D printing and additive manufacturing in industry has grown as well, as new techniques and research result in improvements in the quality of prints. One such example of the various industrial applications of 3D printers include the manufacture of a car chassis [7] and perhaps most notably is innovations in the field of medicine, such as 3D bionics and custom hip implants [8] which are bespoke and made-to-measure for the patient.

The key advantages of 3D printing and the reason it has such an important role to play in the manufacturing sector is because it can be used to manufacture components which conventional manufacturing cannot make. This includes complex shapes which are either too difficult or expensive to mill or machine such as designs with internal cavities or those which do not allow access to areas which need machining. One of the the main areas that has gained traction is rapid prototyping. The nature of 3D printing allows designers the opportunity to print off a physical version of their designs which can aid in design realisation and allow testing before committing manufacturing to a larger scale. It is ideal for lean production, where parts are only produced when required so that no inventory is kept. Additionally, waste is very low as only the material needed for the component is used during manufacture. The next section will go into more detail explaining the whole of the 3D printing process, starting with the digital model and progressing through to the finished component.

1.2 The 3D Printing Process

A key challenge of 3D printing involves the conversion of the digital model to an instruction set which can be printed. This section will now discuss this process.

The typical process of printing a 3D model starts with a 3D digital model. Models are created in Computer Aided Design (CAD) software packages and are exported as Stereolithography (*.stl*) files. *.stl* files describe the surface geometry of the object through polygons. These *.stl* files are then imported into a slicing software package, which is a type of Computer Aided Manufacturing (CAM) package, and sliced. Slicing refers to a process where the package converts the *.stl* file, which is a 3D model, into many 2D horizontal layers, (as previously mentioned around 0.2 mm in height) and generates the instruction set for the 3D printer so it can print off the desired component.

The output generated by slicing packages is known as Gcode, which is a control language used by 3D printers and many other manufacturing machines, including Computer Numerical Control (CNC) milling machines. Gcode is a text file which contains the sequence of commands that will generate the component. The majority of commands contain X, Y and Z coordinates, so the motors can move the print head and print bed to the correct location, in addition to the amount of material to extrude. Other commands set the extrusion temperature and other printer settings.

Slicing packages have an important role to play in taking the digital object from the *.stl* file

and converting it into an object that can be printed. A variety of parameters can be changed during slicing which will change the quality and the characteristics of the final print. These include the layer height, the number of shells, adding supports, the infill type, the infill percentage, the extrusion speed and the extrusion temperature. The number of shells is the total number of external perimeters that will be printed, where two shells are typically chosen. Some of the other parameters listed here will be explained in the remainder of this section.

Figure 2 shows a labelled microscope image of a 3D printed part which explains what some of the terms used in this paper refer to, including shells. The image features two shells, as can be seen by the two sets of arrows labelled C.
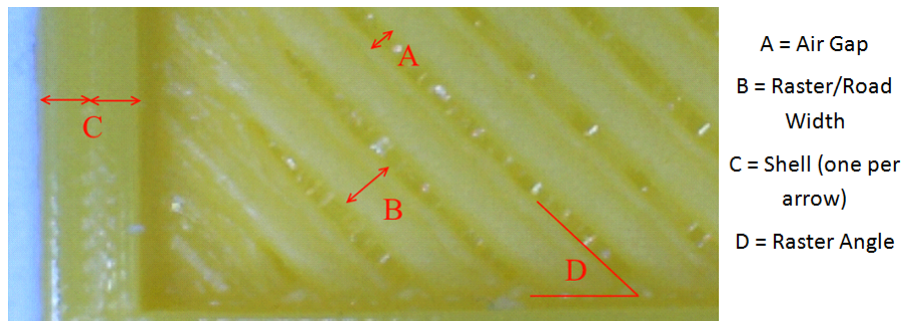
Figure 2: Microscope image of 3D printed part labelling key features.

Support structures can also be included during slicing. These can be necessary because as the model is built up layer by layer vertically, new material is deposited on top of previously deposited material. Therefore if the model has overhangs, there will be no previously deposited material directly below for the new material to sit on top of. Thus simple support structures are included which can be removed once the model has finished printing. Adding support structures does add to the amount of waste during the FDM process. If an object can be reoriented so that support material is not necessary, then material will be saved. An example of support structures has been shown in Figure 3. The rabbit in (a) is as-printed which includes the support material. The support material has been removed to leave the final rabbit model in (b).

Figure 3: Support material before (a) and after removal (b). Reproduced from [2].

To save material and time during printing, slicing packages use a reduced infill inside the printed models. There are a variety of infill patterns available; hexagonal, concentric, rectilinear, Hilbert curve and Archimedean chords to name a few. These are shown in Figure 4.
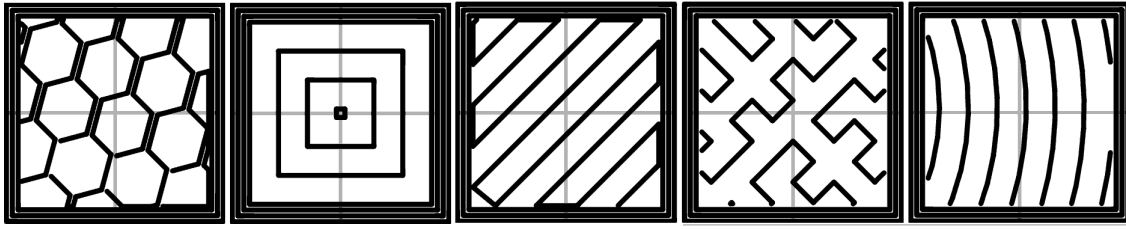
Figure 4: Different infill patterns. From left to right: Hexagonal, Concentric, Rectilinear, Hilbert curve, Archimedean chords. Reproduced from [3].

A commonly used infill pattern used by slicing packages is a hexagonal infill. These hexagonal structures can be of varying infill percentages, as shown in Figure 5, where a higher infill percentage prints more infill material at the expense of taking longer to print. Hexagons are often chosen for the infill pattern as a regular hexagonal grid is the most optimal way to divide a surface into regions of equal area with the least total perimeter according to the honeycomb conjecture [9].
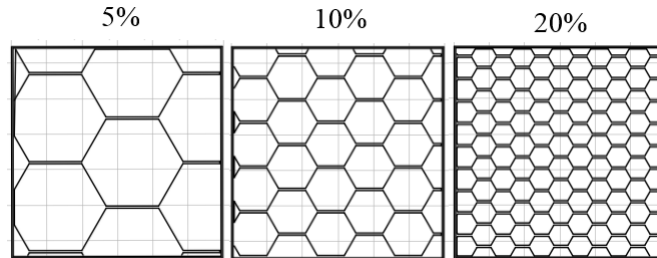
Figure 5: Three different hexagonal infill percentages.

1.3 Challenges of 3D printing

Even with all of its merits, 3D printing is still a research field in its infancy with many opportunities for improvements. Many of these improvements would be to address the variety of challenges facing the users of 3D printers, most of which are listed on the RepRap wiki page [10]. These can be summarised as reliability and repeatability problems, which include filament blockages or warped final components. Other problems are a result of non-optimal slicing settings. This can result in the final piece not being able to support the load it was designed for and failing or the structure being over-engineered, wasting material and print time.

The main factors affecting the strength of the final part are the number of shells used, the infill type and the infill percentage. These are all parameters which the user defines during slicing. Higher infill percentages and more shells result in a stronger part due to more material being used. However, printing more material is more costly and takes longer to print. Therefore research into finding an optimum balance between print times, material usage and strength is key.

At present, when slicing with slicing packages, users manually select the infill percentage used as well as selecting the layer height and number of shells. An example of commonly used settings is selecting two shells and a 10% infill, because these are the default settings for many common slicing packages and are empirical derived. Users will either print a part with too much infill, which wastes plastic and print time, or they will print a part with not enough infill, which is likely to fail during operation and again will represent a waste in plastic and print time.

Thus there exists an opportunity to develop an automatic, efficient way to create an optimum infill design based on the loading conditions and requirements of the 3D printed part. In

industry, wasted plastic and lost print time means money will be lost. Therefore there is an economic incentive to optimise the infill of 3D printed components based on the specific loading conditions that they will experience. Selecting slicing settings is more guesswork as opposed to a science at present and this acts as a barrier to industry-wide 3D printing use. An efficient and reliable method to optimise infills will help remove these barriers.

1.4 Aims and objectives

The previous section has highlighted a number of opportunities for further research. The main aim of this research is to develop and investigate a strategy for generating and printing an optimised infill design for 3D printed components. The optimisation is based on the loading conditions of the part to improve its performance when considering two specific metrics: strength-to-weight and strength-to-print-time.

In order to meet this aim, the research has been organised into 2 objectives. The first objective was to develop a strategy that will design and print an optimised infill design for a structure with any loading conditions.

The second objective was to evaluate the performance of a specific load case; a rectangular section beam under three point loading conditions. The optimised designs were printed and tested against standard hexagonally infilled beams. For the strategy to be successful, the metrics for the optimised beams should be higher than the metrics for the standard beams.

The future potential of this work is to offer an infill optimiser inside an FE (Finite Element) package, where the user only has to input the location and magnitude of the forces the component will experience and the software will calculate an optimal infill pattern and slice the model ready for printing. With the work presented in this paper, 3D printing will be able to be used in more industrial applications and used for engineering structures where strength-to-weight ratios are very important; in aircraft wings for example. It will also bring analysis into the design process.

This paper continues by presenting a literature review of the work done by others in the areas of 3D print optimisation and topology optimisation. This is then followed by an explanation of the strategy developed to optimise infill designs for 3D prints. The paper will then describe the testing process used to demonstrate the implementation of the strategy developed and present the results of these tests. A discussion will follow which will investigate the method used, the results, and discuss further work. The paper will finish with a conclusion of this research and its key findings.

2 Literature review

This section features a literature review of current work. The result of the main aim of this project was to improve the strength-to-weight and strength-to-print-time metrics for 3D printed parts through topology optimisation. Therefore this literature review features previous works concerned with either improving the strength of 3D printed components or topology optimisation. This literature review has been organised into three research areas. The first is the optimisation of 3D printers to improve the mechanical properties of printed components. The second is the area of topology optimisation, with considerations for topology optimisation in regards to infill optimisation. The third section of this literature review discusses the advantages and disadvantages of current commercial packages for slicing and topology optimisation.

2.1 Optimisation of 3D Printed Components

The mechanical properties of 3D printed mediums differ greatly compared to the same material which has been cast or injection moulded. This is because 3D printed parts are made up of lots of very thin layers bonded together as opposed to a single structure. This results in 3D printed parts being less mechanically strong than their cast counterparts. It has been found that the meso-structure of 3D printed ABS parts causes the elastic modulus to be 11 to 37% lower and the strength values to be 22 to 57% less than injection moulded ABS [11]. However, even though 3D printed components are not as mechanically strong as subtractive-manufactured parts, they can still be considered mechanically functional. The tensile strength of printed PLA has been calculated to be 56.6MPa with an average elastic modulus of 3368MPa [12]. These values show that 3D printed components can be used as substitutes to subtractively-manufactured components. 3D printed parts also demonstrate anisotropic properties due to the way layers and rasters are printed [13]. Thus the strength and other mechanical properties vary in different directions depending on the orientation the material has been deposited in.

A variety of studies have been performed to either calculate the effects of changing slicing settings such as layer thickness and raster orientation on the mechanical properties of 3D printed components. Other work includes the development of algorithms to improve these mechanical properties. The next section discusses these studies.

Mechanical Properties As the strength of 3D printed components plays a very significant role in this research, a discussion of the factors which affect the strength of these components follows.

Layer thickness has an important role to play in determining the mechanical properties of the final 3D printed component. It has been shown that as layer thickness increases, the maximum flexural force of 3D printed parts tested in a 3 point bend test decreases. Luzanin et al. showed that there is a dominant, statistically significant relationship between these parameters, as demonstrated through an analysis of variance [14]. The ultimate tensile strength has also been shown to decrease with increasing raster angle [11].

The elastic properties of 3D printed components have been tested though the use of 3D printed members in a catapult design. It was shown that the three parameters layer thickness, raster angle and air gap made a significant difference to the elastic properties of the 3D printed members [15]. Increasing these three parameters resulted in increasing the catapults average throwing distance. These three parameters were shown to have a contribution of around 30% each in the analysis of variance, whereas raster width only had around a 5% significance.

Print temperature is another slicing setting which can be modified. However, a Design of Experiments method was used to show that changing the print temperature does not have a significant effect on the ultimate tensile strength of the test pieces [13].

Due to the nature of the process of 3D printing, air gaps form between the raster roads. It was found that the air gap between raster roads had the greatest influence on the wear strength of the printed parts at a 95% confidence level [16]. Thus there exists an algorithm which aims to reduce the air gaps in printed components. The method aims to improve the tensile properties of 3D printed parts by using a visual method to try and eliminate air gaps between rasters. Improvements of as much as 19% were achieved in ultimate tensile strength compared to the default build parameters [17].

Another algorithm developed optimises the orientation of 3D printed parts to increase their tensile strength using adaptive slicing [18]. The algorithm analyses the cross-sections of a structure to find the highest stressed areas and re-orients the model into a different plane to

increase the amount of material in these areas and thus increase the parts mechanical strength when printed. The next section investigates topology optimisation and previous work in the area of topology optimisation of 3D printed components.

2.2 Topology Optimisation

3D printing is well suited to manufacture topology-optimised components because topology optimisation often creates organic shapes that are hard to create using traditional manufacturing techniques. There currently exists a wealth of work in the field of topology optimisation for subtractive manufacturing [19]. However, topology optimisation for additive manufacturing has not been researched in as much depth. A reason for this is that conventional topology optimisation tools start with a solid billet and remove material until an optimal amount of material remains. This suits subtractive manufacturing, as the subtractive manufacturing process removes material to create a final component. However, additive manufacturing adds material to create a final component, and so a topology optimisation process which adds material during each iteration of the optimisation would be better suited towards additive manufacturing.

A further problem with topology optimisation is that it can optimise a structure and present the results on a computer screen, but the challenge is actually manufacturing that optimised, theoretical result. These challenges have been summarised by Zhou et al., where the design requirements for casting and extrusion production have been considered for topology optimisation [20].

An additive-manufactured aircraft hinge bracket has been topologically optimised to save weight and cost [21]. The lack of economic viability of the optimisation process was noted due to the high number of man hours required. It was concluded that the process would become more economically viable if optimisation tools for additive manufacturing had been developed. Brackett et al. discussed a variety of issues regarding the application of topology optimisation for additive manufacturing methods [22]. The main areas that were investigated included the manufacturing constraints which must be considered when performing topology optimisation and adding support structures into the optimisation process. It was concluded that even though topology optimisation is in its infancy, there exists great potential for its development and use in industry.

There also exists a method developed with similar aims to that of this research. The method optimised the strength to weight ratios of 3D printed parts by modifying their internal structure [23]. The method is based on an irregular hexagonal cell structure. A Voronoi diagram is utilised to generate the irregular hexagonal internal structure of a 3D model based on the stresses in the model as a result of a defined external force. An optimisation sequence is then used to remove as much material as possible from each hexagonal cell to maximise the strength-to-weight ratio based on given loads applied to the model. The method goes through numerous iterations to reach a final, optimised model based on strength-to-weight ratios. The irregular honeycomb-like structure that this method produces is not optimised for ease-of-printing because the printer will have to make lots of small, non-continuous print moves which is much slower than long, continuous print movements. Additionally, the method is quite computationally intensive compared to the method proposed in this paper.

Furthermore, the method uses a Monte Carlo simulation which will not result in exactly the same topology each time. This means that if the process was ran numerous times for exactly the same inputs, the orientation of the hexagons would be slightly different each time. This would result in final printed components with slight differences in strength due to differences in orientation of the printed material. Moreover, the method uses a subtractive iteration process

where material is removed during each iteration until an optimum infill pattern is reached. This suits subtractive manufacturing, but is not ideal for additive manufacturing. The method has not been incorporated in industry or has not been developed into an easy-to-use commercial package. Thus the need for a usable process to optimise internal structure still remains. The next section discusses the advantages and disadvantages of two commercial slicing and optimisation software packages.

2.3 Commercial Packages

There exists a commercial slicing package, Simplify3D, which allows users a lot of freedom when slicing [24]. The main benefit of this software is that it allows users to select different regions of their 3D CAD model and change the infill percentage in these different regions. This means that users can put higher infill percentages in higher stressed areas and reduce infill in less stressed areas. However, this software requires manual expertise and does not incorporate any intelligent process to do this automatically. Therefore it is an improvement to standard slicing packages which only allow one infill percentage for the entire model, but it does not feature any automatic way to optimise the infill. Additionally, users can only use the standard infill patterns offered (see Figure 2) and change the local infill percentage of these patterns in a model. There are no custom infill patterns which are designed specifically to the model and its loading conditions.

A second commercial package available, Altair Optistruct, is an optimisation package with a variety of features, including topology optimisation. In a recent update, the topology optimisation suite has been expanded to support the use of 3D printing so that it can create a mix of lattice and solid sections, which are suited to the 3D printing process [25].

However, this software package will not create a 3D printable file which can be printed on a 3D printer. It simply generates the optimised design based on input parameters defined by the user. A key consideration when creating 3D print files is if it is possible to print the geometry that has been created. For example, shapes with internal overhangs are likely to need extra supports which the topology optimiser will not include. Optistruct does not consider if the geometry generated will be printable. Thus there is a need to incorporate these sorts of technologies with a program which can generate printable files.

Table 1 summarises the key statements from this literature review in regards to the effects changing certain slicing parameters has on the printed components strength and the time taken to print. The statements made in the table are either based on the referenced work from the literature review or are logical conclusions based on these works.

	Print Time	Strength
Increase layer height	Significantly decrease	Significantly decrease
More shells	Significantly increase	Significantly increase
Include supports	Significantly increase	No effect
Higher infill %	Significantly increase	Significantly increase

Table 1: Table summarising effects of changing 3D printing parameters on final print.

3 Objective 1 - The Optimisation Strategy

This section discusses the methods which were considered when developing the optimisation strategy and then describes the method chosen in detail.

3.1 Choice of Method

Two alternate methods, Methods 1 and 2, were considered when deciding which approach to take to develop the strategy to optimise infill patterns. These methods were not selected and an outline as to why has been given. Following this explanation, a description of the method used has been given.

Method 1 The first option considered was to take results from FEA where the stress distribution across the beam was calculated based on the loading conditions applied. This stress distribution would then be used to create different sized hexagons, where smaller hexagons, and thus more material, would be placed in areas of higher stress, and areas that are less stressed would have larger hexagons. This method is similar to that used by Jin et al [23], except that they performed numerous iterations to find the optimal irregular hexagonal grid layout. This method optimised the entire 3D structure and thus needed many iterations to get an optimised result.

Method 2 The second option considered involved taking the hollow shell of the component and generating solid struts along the force paths calculated from FEA. These solid struts would help transfer the load through the part and support the load applied. This method involves 3D analysis and is thus more computationally intensive than a 2D analysis.

Method Reasoning The reason Method 1 was not chosen was because generating an irregular pattern of hexagons would have taken longer to print due to the printer starting and stopping extrusion and not performing fast, continuous travel moves. The aim of this research was to optimise 3D prints for strength per unit of weight and printing time and thus this was not deemed to be a viable option due to the increase in time taken to print. Method 2 was not chosen because it would only have material along the force paths and very little or no material in other areas. The lack of a regular grid would not help transfer load very well and would not be successful for complex loading conditions or structures, which will require spider-web-like strut-systems to support the load. These complex strut-systems will be very computationally intensive to generate. The next section details the method chosen for the strategy with the aid of a flow chart. The advantages and disadvantages of the method chosen have been discussed in the Discussion section of this paper in Section 7.3.

3.2 Method Chosen

This paragraph briefly discusses a flow chart, shown in Figure 6, which shows the key stages of the strategy developed in this research. The strategy commences by performing FEA (Finite Element Analysis) on the component based on its loading conditions. This will create a stress distribution which is imported into MATLAB. This stress distribution is then used to design the infill pattern of the component. A rectangular grid is set up inside the component and cells in this grid with a stress above certain values will be infilled with more material. The instruction set for the printer based on this grid and infill pattern is written to a text file. This text file can then be converted to a printable file and printed on the 3D printed. The next section will now explain the strategy and the flow chart in more detail, making reference to the numbered elements in the flow chart.
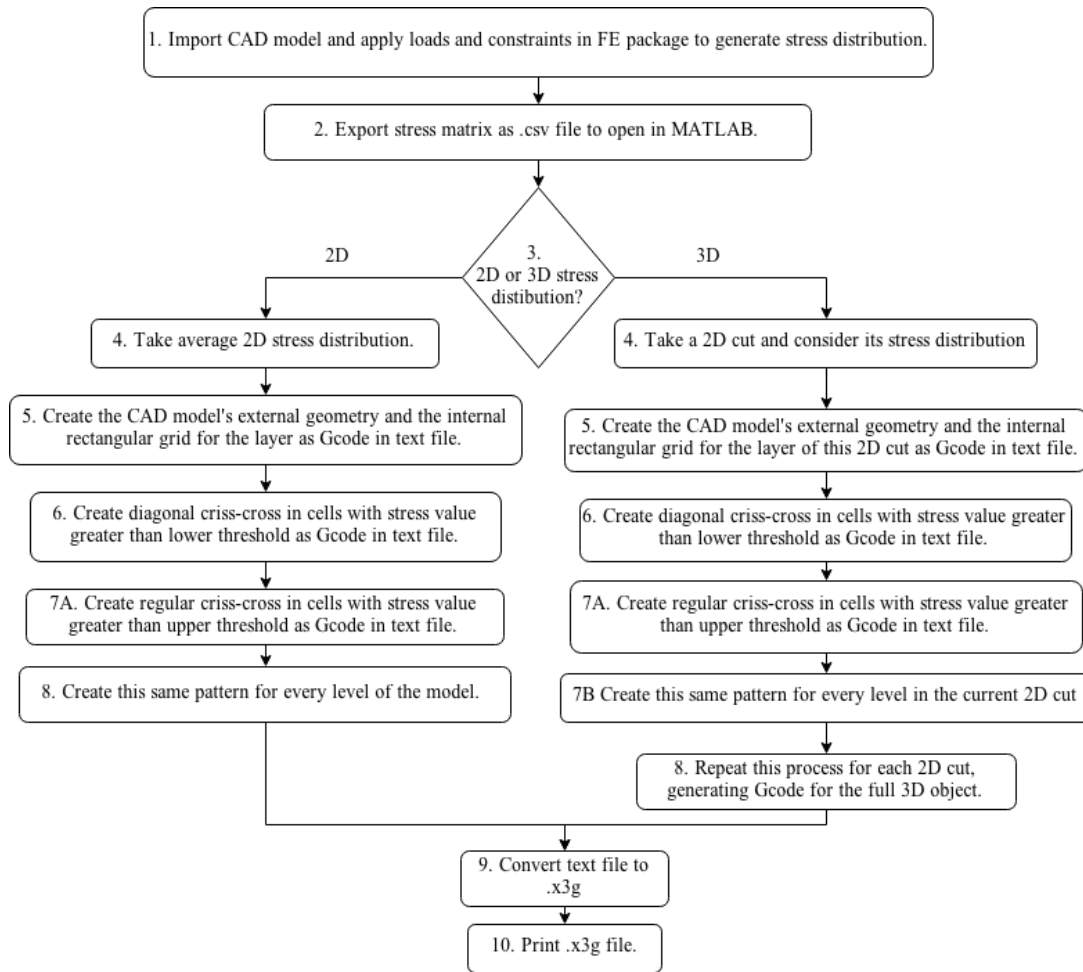
Figure 6: Flow diagram of optimisation process.

3.3 Using the FEA package - Flowchart Elements 1 & 2

The purpose of using FEA is to evaluate the stress distribution across the component based on its loading conditions which will be used to design the infill pattern. This section describes how this distribution is found. Autodesk Simulation Mechanical was the FE (Finite Element) package selected for this strategy as it allowed exportation of the stress distribution of the model as a *.csv* (Comma-Seperated Variables) file. Any FE package can be used however as long as the stress distribution of the model can be exported.

The first step of the strategy is for the user to import the *.stl* file of the CAD model into the FE package (flow chart element 1). FEA works by splitting up a model into a fine mesh of very small volumes over which stress analysis is performed. The first stage of the FEA is to mesh the model. The infill pattern used in this strategy is based upon a regular rectangular grid and thus, to simplify the process, the current method is constrained to used a regular cuboid mesh in the FEA. The reason for this is because the FEA cuboid mesh is directly mapped to the printed infill grid used. Therefore the size of the mesh used in the FEA package is the same size as the size of the rectangular grid used in the infill pattern design. So, choosing a finer mesh with more squares will result in a finer infill mesh.

The user must then apply the loading conditions and constraints to the model in the FEA package based on the loading conditions the printed component will experience. This includes

constraining certain faces of the model which are known to not be allowed to move; for example the built in face of a cantilever beam. The loads applied can be in the form of pressures, point loads or moments.

The stress analysis can then be performed, which will output a stress distribution. Figure 7 shows the von Mises stress distribution resulting from a rectangular section beam loaded under 3 point loading conditions. This rectangular section beam is the beam chosen as the proof-of-concept for the strategy developed in this research. The beam has a length of 180 mm, a height of 60 mm and a depth of 20 mm. The simple supports are 120 mm from one another. This stress distribution is then exported as a *.csv* file to MATLAB (flow chart element 2).
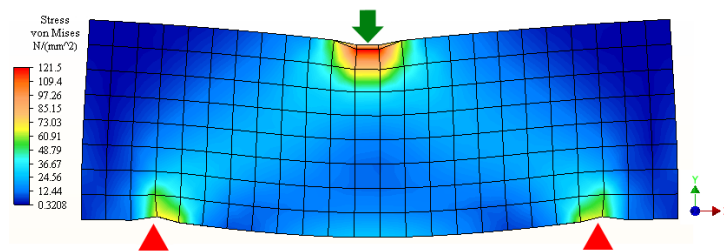

Figure 7: von Mises stress contour plot of beam under 3 point bending conditions, showing simple supports (red triangles) and point load (green arrow).

3.4 Importing into MATLAB - Flowchart Elements 3, 4 & 5

The MATLAB code developed for this strategy will import the *.csv* file generated by the FEA program and convert it into a 4-columned matrix which contains the X, Y and Z coordinates and the stress value for each node from the FEA model. The nodes of the model are the points between which the lines of the FEA mesh connect. The elements in an FEA mesh are 3D volumes and in this case the elements are cubes, where each is made up of 8 nodes, one at each corner. The 8 nodes of every element are listed in this *.csv* file which therefore includes a lot of repeated nodes as nodes are shared between elements. The repeated nodes are removed so that each node is only represented once in the matrix. The MATLAB function *insertrows.m* was downloaded and used to help remove the unwanted repeated nodes [26]. This resulted in a matrix which contained the stress distribution for every node of the model in all 3 dimensions.

The program then splits this matrix up into 2D cuts and decides if the stress distribution through the beam is 2D or 3D (flow chart element 3). Each 2D cut is defined as an X-Y plane of nodes, where every node in the cut has the same Z coordinate. The Z direction is the direction going into the page in Figure 7 and the X and Y directions are shown in the Figure. If the stress distribution in the component is 2D, then the stress distribution is the same in all of the 2D cuts. The beam shown in Figure 7 has a 2D stress distribution as every 2D cut, or X-Y plane, has the same stress distribution due to the symmetrical nature of the 3 point bend test. A 3D stress distribution will have a different stress distribution for each 2D cut. The difference between the 2D and 3D stress distributions is that the beam with a 2D stress distribution is only made up of one 2D cut, whereas the beam with a 3D stress distribution is made up of multiple, smaller 2D cuts, each with its own stress distribution. The following explanation will explain the process for a component with a 2D stress distribution. It will follow with a paragraph explaining how the process differs for a 3D stress distribution.

For a 2D stress distribution, the average 2D stress distribution of all the 2D cuts of the beam will be calculated and stored as a new 2D matrix (flow chart element 4). This new matrix of nodal stress values can be plotted and is shown in Figure 8 for the three point bended beam. It

can be seen that the contour plot in Figure 8 is very similar to that in Figure 7 which shows this method works correctly.
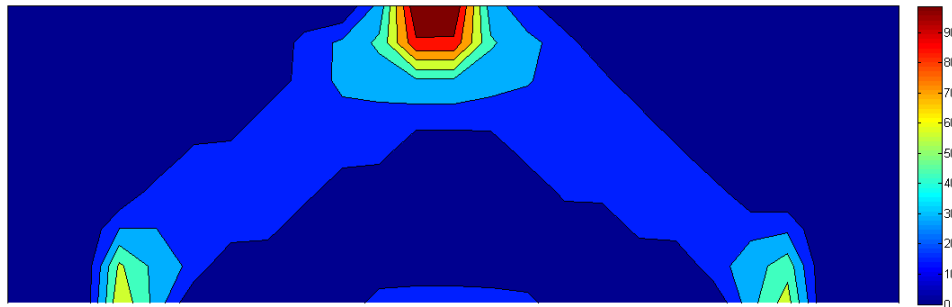

Figure 8: Filled contour plot showing the imported von Mises stress distribution for the three point bended beam (Colour bar units MPa).

The user must then enter the dimensions of the beam into the MATLAB program. The program will then generate the Gcode for the outer geometry and write it to a text file (flow chart element 5). It will also generate the rectangular grid in Gcode and write this to the text file as well. This is the start of the infill optimisation. The next part of the program will be used to decide which cells in this grid need more material added and which do not based on the amount of stress in the equivalent part of the beam in the FEA model.

3.5   Performing Iterations - Flowchart Elements 6, 7 & 8

In the next part of the strategy, the MATLAB program will perform iterations to add material to certain cells in the grid. The nodes of the FEA model are located such that they lie at the centre of each cell in the printed infill grid. Two threshold stress values are calculated, where cells in the grid with stress values lower than the lower threshold stress value will not have any material added. Cells with a stress value above the lower threshold will have two cross members added. Cells above the upper threshold will have a star pattern added. Figure 9 shows the three different levels of infill for a single cell.
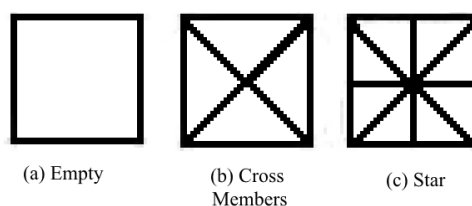
Figure 9: The three levels of infill used in the optimisation process.

The reason the two cross members were chosen for the first infill level is that firstly they add material in a different direction to the rectangular grid which increases stiffness and strength in different directions. Secondly, the two cross members only require 3 moves to print per cell. This is fewer moves than the star pattern, which takes 6 moves to print per square. The star patten is not used as often as the two cross members but is used to add extra strength to the cells which are the most highly stressed. If the amount of material in the empty cell, including the four edges of the cell, is assigned a value of 1, then the amount of material in the cross-membered cell is 1.7 and the amount of material in the start patterned cell is 2.2.

The threshold stress values were calculated by considering the stress at every point in the matrix and organising the stress values into rank order. The stress at the 20th percentile of this

order is defined as being the upper threshold stress and the stress at the 70th percentile of this order is defined as being the lower threshold value,

The first optimisation iteration involves creating the Gcode to add the cross-member pattern to cells in the grid with stress values above the lower threshold value (flow chart element 6). The second optimisation iteration involves creating the Gcode to add the star pattern to cells in the grid with stress values above the upper threshold value. Thus, cells with higher values of stress have more material added to them (flow chart element 7A). Once this process is complete, this finishes the optimisation for components with the 2D stress distribution case. The Gcode generated for this 2D cut is repeated for every layer in the beam (flow chart element 8).

3D Stress Distribution   For the 3D stress distribution the process is slightly longer. The beam is split into multiple 2D cuts. Then each of these 2D cuts undergoes the same process mentioned above regarding adding the cross-member and star patterns to add material to the higher stressed areas. The only difference is that once the optimised pattern has been generated for the first 2D cut, the Gcode is only generated for layers included in that 2D cut (flow chart element 7B). Then the next 2D cut is taken and optimised in the same way, generating Gcode for the layers in that 2D cut. Once all of the 2D cuts have been analysed, then the Gcode is finished (see flow chart element 8).

3.6   Converting and Printing - Flowchart Elements 9 & 10

All of the Gcode created in the previous section in MATLAB gets written to a text file. Once the optimisation is finished, then this text file containing Gcode can be converted into an *.x3g* file (flow chart element 9). An *.x3g* file is a binary version of Gcode which can be read by 3D printers. Dr Henry Thomas's Gcode-to-*.x3g* converter, *GPX* was downloaded and used to convert the text files containing the optimised Gcode [27]. The *.x3g* file which has now been created can then be uploaded to the 3D printer and printed off (flow chart element 10).

4   Objective 2 - Evaluating the Strategy

The strategy developed in this research is capable of generating optimised infill patterns for any beam dimensions and any loading conditions. To demonstrate the wider applicability of this strategy, a rectangular section beam under 3 point bending conditions was optimised and tested against non-optimised hexagonally-infilled beams.

4.1   Three Point Bend Test

The optimised beams and the hexagonally infilled beams were tested under 3 point bend conditions and the flexural strength of the beams was measured. Every beam was printed out 3 times and the average results were taken to ensure reliability. The separation of the simple supports was 120 mm which matches where the supports were placed on the FEA model. The simple supports were not placed at the end of the beams to prevent the beams from slipping during testing.

All the beams were loaded at 100 N/minute until fracture or until the maximum loading capacity of the machine was met. The software connected to the loading machines plotted graphs of force against extension and provided a *.csv* file which contained this data. The force required to reach yield stress was the parameter used to assess the flexural strength of the beams.

The 0.2% strain method was used as it is often very hard to identify the end of the linear region and thus the transition from elastic behaviour to plastic behaviour.

The key parameters which were measured and used to compare the beams were the strength-to-weight and the strength-to-print-time ratios of the beams. Once the force to reach the yield point was identified, then the first metric, strength-to-weight ratio, was calculated by dividing the yield force, in Newtons, by the weight of the beam, in grams. The second metric was then calculated, where the yield force, in Newtons, was divided by the time taken to print the beam, in minutes. The aim of the optimisation process was to create beams which scored higher in terms of these two metrics, i.e. having a higher strength per unit weight or per unit print time.

Two machines were used to apply the compressive force required for the 3 point bend test. The first machine used was the Instron 3343 1KN Single Column Testing System. It was fitted with an Instron 2519-105 1KN load cell. The load cell had linearity and repeatability ratings of 0.25% [28] and an accuracy of 0.5% [29] of the maximum load. The second machine used was the Zwick Roell HCT 25KN. This machine was capable of applying a force of up to 25KN and was hydraulically powered. The reason for using this second machine is that, during testing, it became apparent that some of the heavier beams could be subjected to the 1KN maximum load and still remain in their linear, elastic region and thus not reach the 0.2% yield point. Therefore, the heavier beams, including some of the optimised beams, had to be tested on the Zwick Roell as this could apply a much higher force which allowed the yield point of these heavier beams to be reached. The next section describes the hexagonally-infilled beams tested and the dimensions of the test pieces.

4.2   Beams Tested

A variety of hexagonally-infilled beams were tested to provide a benchmark to compare to the optimised beams. A hexagonal infill was chosen as it is the default infill on slicing packages, such as MakerWare, which is the in-house slicing package for the MakerBot Replicator 2. The infill percentages chosen were 5%, 10%, 15% and 20% because these are common infill percentages used and make up the default options for MakerWare. Figure 10 shows a render of each of these beams. The Figure in Appendix 10.1 shows a render of the eight different infill patterns used in the testing, including the optimised beams. The dimensions and print settings used to generate these beams have been detailed in the next section.

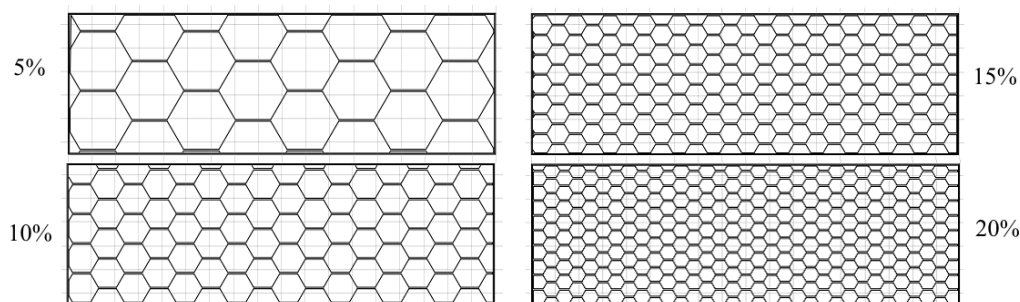Figure 10: Renders of the four types of hexagonal infill percentages used.

Materials and Dimensions   The 3D printer used was the Makerbot Desktop 2, which has a build envelope of 285 mm by 153 mm by 155 mm (length, height, depth). The filament used was Makerbot PLA filament. It has a diameter of 1.75 mm, a density of 1250 Kg/m^3 [30] and a melting point of 170 °C [31]. The only parameter which was changed when printing was

the internal structure of the beams. Each beam had a length of 180 mm, a height of 60 mm and a depth of 20 mm. In the paper by Eschenauer & Olhoff, the optimum topology solution to a 3 point bend test on a rectangular-section beam was calculated [32]. The length to height ratio (3:1) from that paper was used for the beams in this. With this ratio selected, the height of 60 mm was chosen as it allowed for two beams to be printed at the same time on the print bed which was favourable in terms of printing as more beams could be printed simultaneously. Thus the length of 180 mm was selected as it follows on from the 3:1 ratio based on the 60 mm width. The depth was chosen to be 20 mm as if the depth was less than this, then there would have been a risk that the beams would buckle immediately under the load applied and would not provide useful data to prove the concept developed in this paper. Furthermore, if the depth selected was too high, then each beam would take longer to print, so a compromise of 20 mm was selected.

The dimensions chosen for this beam were relatively arbitrary as the only imposed constraints were the build envelope of the 3D printer. This differs greatly to industry, where the height chosen is of considerable importance, where height constraints dictate beam dimensions, such as in floor joists in buildings where there is a maximum allowable height for the joists. It has been shown that the height constraint of a beam has a significant effect on the optimal shape of the beam as the optimum shape, or in this case infill, of the beam is not always the same as the optimum shape for the unconstrained beam [33].

Slicing settings For the purposes of testing, the top and bottom faces of the beams were not printed so that the internal structure of the beams could be seen clearly during testing. This also reduced the time taken to print each beam by 43 minutes, which was a significant saving. MatterControl was the slicing package used to create the hexagonally-infilled beams and Slic3r was the slicing tool selected. MakerWare, which is the in-house slicing package for the MakerBot, was originally the program used. However, it was not possible to print the beams without the top or bottom faces in MakerWare. Thus MatterControl was used to slice the beams and to generate the print files as it had the facility to print the beams without the top or bottom faces.

The layer heights used were 0.2 mm throughout and the temperature the filament was heated to was 230 °C. All prints were in the same orientation, with the same raster angle (-45 °/45 °). No rafts or support material was printed for the beams as they were unnecessary. Each beam had two shells.

The printer moves the print head at different speeds depending on if it is extruding material or if it performing a travel move, where it moves to the next position but does not extrude any material. The printing speed was 90 mm/s and the travel move speed was 150 mm/s. The printing speed is slower than the travel move speed as if the printer head moves too quickly whilst extruding material, the material may not deposit correctly and the layers will not bind as they should.

5   Results 1 - Optimised Beams

This section presents the optimised beams generated by the optimisation strategy developed. It also presents the optimisation results for a cantilever beam with a 3D stress distribution.

5.1 Three Point Bend Test Optimisation

This results section deals with presenting the two different optimised beams developed using the strategy discussed in this paper. Using the stress distribution generated in Figure 7, the optimisation process as described above was implemented. The first optimised beam that was generated, designated as 3*Levels* is shown in Figure 11. It received this designation because it features three levels of refinement as seen in Figure 9; the first being the regular square grid, the second being the two cross members, and the third being the star pattern. The material placement in this beam closely resembles the optimum solution to a 2D rectangular beam under 3 point bending conditions calculated by Eschenauer & Olhoff [32].
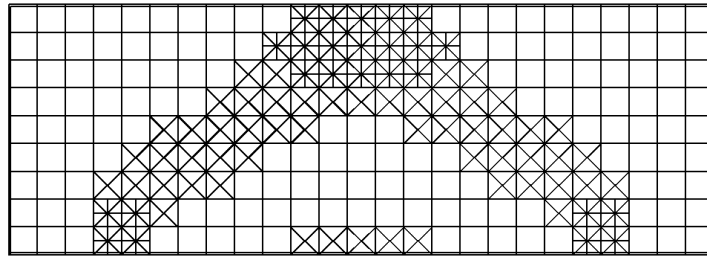

Figure 11: Render of the optimised beam 3*Levels*.

The second optimised beam created was designated *Even*3 and is shown in Figure 12. The aim when creating this beam was to reduce some of the redundancy in the structure by removing some unnecessary material from 3*Levels*. This resulted in it being lighter, but with a similar strength, thus improving its strength-to-weight metric. Some settings in the FEA package were modified to generate this. The same loading conditions, dimensions and constraints were all applied as before. However, the mesh size was adjusted slightly to be one element smaller in both the X and Y directions which resulted in an even number of cells in the optimised infill grid. This allowed for the possibility of only printing every other line in the grid, which reduced the total weight of the beam. This is evident when comparing Figures 11 and 12. The reason this optimised beam received the designation *Even*3 is because it had an even grid spacing and has 3 levels of refinement.
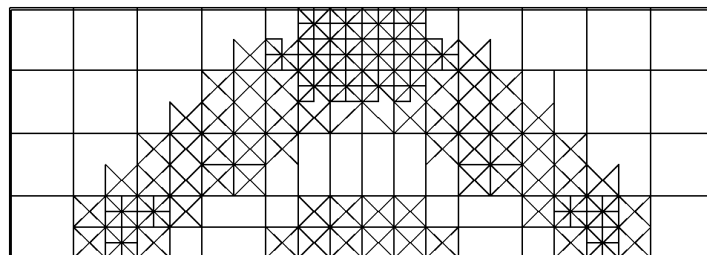
Figure 12: Render of the optimised beam *Even*3.

5.2 3D Stress Distribution Optimisation

A beam with a 3D stress distribution was also optimised using the strategy presented in this research. The dimensions of the beam were changed relative to the other optimised beams to show the flexibility of the MATLAB program. It was a cantilevered, rectangular-section beam and had a length of 120 mm, a width of 50 mm and a depth of 20 mm. The beams smallest face (Face A) was fixed and a uniform force was applied to the top face (Face B) and one of the side faces (Face C). The stress distribution calculate by the FEA has been shown in Figure

13. It can be seen that the stress distribution is 3D, as the stress distribution changes along the beams Z-axis.

Figure 13: FEA stress distribution of the cantilever beam.

Figure 14 shows the four 2D cuts of the cantilevered beam generated by the optimisation strategy. The number of each cut relates to the relevant layer of the beam shown in Figure 13. The MATLAB program used the stress distribution from each cut to create the Gcode for each cut, where each cut is one quarter of t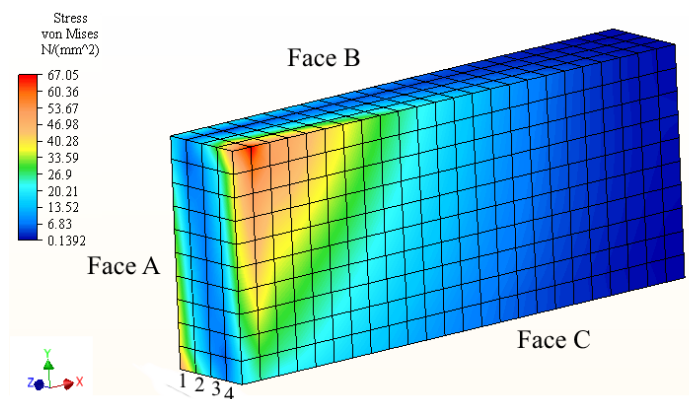he total depth of the beam. Therefore when the beam is printed, each 2D cut will have a different infill pattern. This differs to the beams optimised earlier in this paper, which had a 2D stress distribution and thus the infill pattern was constant through the depth of the beam.
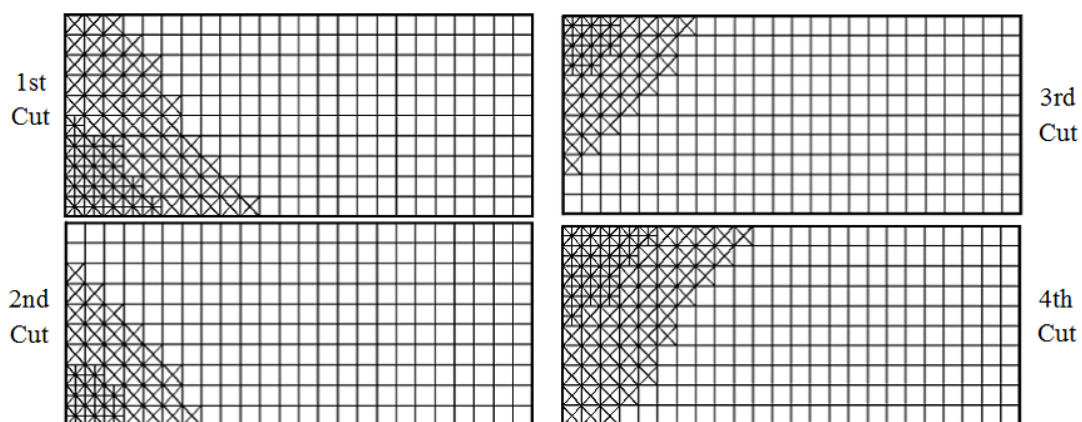
Figure 14: Renders of the four 2D cuts of the optimised beam.

6 Results 2 - Testing

This section presents the results of the 3 point bend test and compares the metrics calculated for the hexagonally infilled beams and the optimised beams.

Figure 15 shows a bar graph plotting the average strength-to-weight ratio and average strength-to-print-time ratio calculated for the beams tested. The full table of results has been included in Appendix 10.2 and the average force-extension graphs for all the beams is shown in Appendix 10.3. The results for the four hexagonally-infilled beams are plotted in Figure 15 (a), and include the 5%, 10%, 15% and 20% beams. The results shown in Figure 15 (b) represent the optimised beams which were created. The beam 1*Level* is the simple rectangular grid as in Figure 11 but without either the cross-member or star patterns. The beam *Even*2 is similar

to *Even*3 which was shown in Figure 12, but it only contained two levels of refinement and therefore did not contain the star patterns at the points of the highest stress. These two extra beams were printed and tested to demonstrate the increase in the strength-to-weight metric by adding material in the areas of high stress. The equivalent infill percentages of the optimised beams have been shown in brackets in Figure 15 (b).

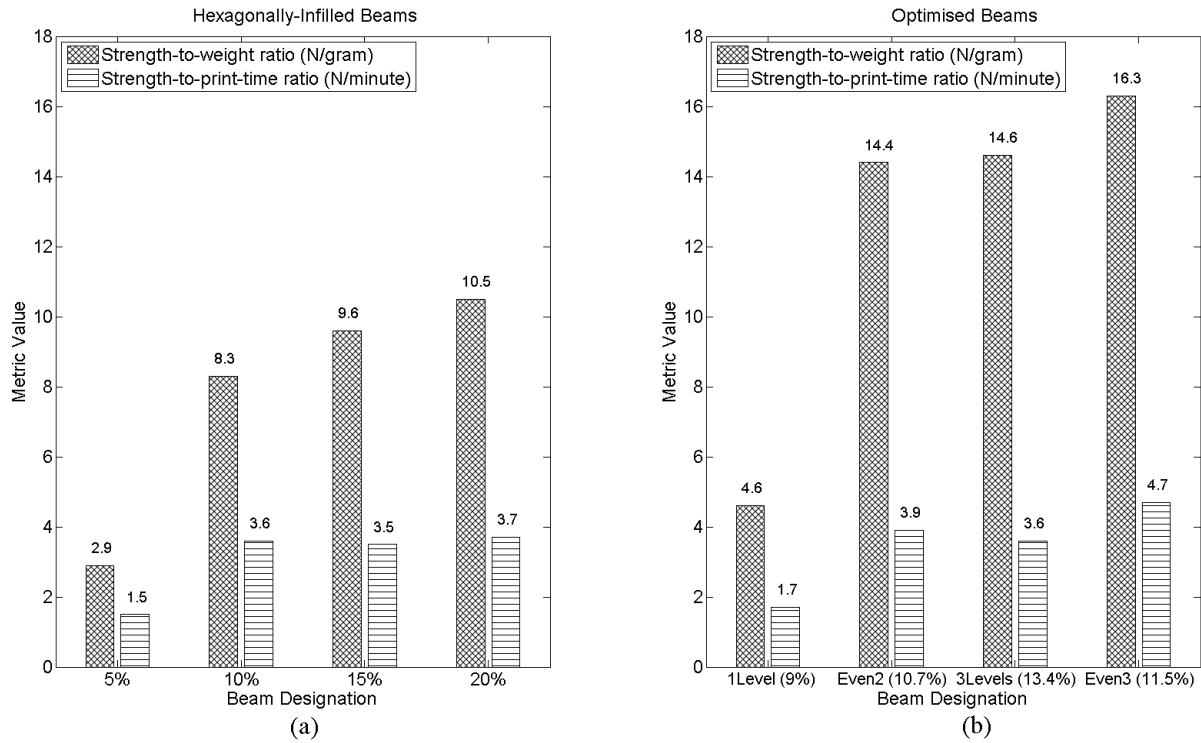Figure 15: Bar graphs showing the calculated metrics of the (a) hexagonally-infilled beams and (b) the optimised beams. Equivalent infill percentages of beams in brackets.

It is clear to see from Figure 15 that the optimised beams outperformed the hexagonally-infilled beams in terms of the strength-to-weight metric. The best performing beam, *Even*3, scored 16.3 N/gram which is a 55% increase on the best performing hexagonally-infilled beam, 20%, which scored 10.5 N/gram. There is a significant increase in strength-to-weight from 1*Level* to 3*Levels*, which shows that the optimisation process has been successful and has resulted in improved beams. The other metric, strength-to-print-time increased from a maximum of 3.7 N/minute for the 20% beam to 4.7 N/minute for *Even*3, which is a 27% improvement.

The equivalent infill percentages of 1*Level*, *Even*2, 3*Levels* and *Even*3 are 9.0%, 10.7%, 13.4% and 11.5%. These equivalent percentages were found by calculating the ratio of the weight of each optimised beam to the weight of 10% beam. These equivalent percentages demonstrate the high increase in performance that the optimised beams have over the hexgaonally-infilled beams. This is because *Even*2 and *Even*3 only have slightly more material in them than the 10% hexagonally infilled beam, but they drastically outperform the 10% beam. *Even*2 and *Even*3 have a lower equivalent infill percentage than 3*Levels* as they are lighter.

7 Discussion

This section will discuss the results presented in this paper, discuss their reliability and the advantages and disadvantages of the method used.

7.1 Interpretation of Results

The results shown in Figure 15 show that the optimisation strategy developed in this research is successful in improving the rectangular section beams operating under three point loading conditions in terms of the two metrics. Firstly, the hexagonally-infilled beams will be discussed. The heavier three of these beams, the 10%, 15% and 20% all had similar very similar scores for the strength-to-print-time metric, with scores of 3.6, 3.5 and 3.7 N/minute respectively. The reason for this is that the only difference between these three beams is that the infill pattern has been scaled up to include more material as the percentage infill of the beams increases. Therefore, material is deposited by the 3D printer at a very similar rate for each of these three beams. This means that the strength-to-print-time ratios for these beams should be similar as adding more material takes more time but supports more load. It would therefore appear that there exists some linear behaviour between the print time and the flexural strength of the hexagonally-infilled beams. These three beams also had scores which were fairly similar for the strength-to-weight metric of 8.3, 9.6 and 10.5 N/gram respectively, which occurs for a similar reason. The standard deviation of the results for each beam was low and so was not shown on the bar graphs.

5% Beam Conversely, the metrics calculated for the 5% beam were much lower than those of the higher-percentage hexagonal beams, as can be seen from Figure 15 (a). The reason for this is that due to the nature of the three point bend test, the area of highest stress during testing is the area directly below the central loading pin. Therefore these are the cells which buckle first during testing. The 5% beam, when compared to the other beams in Figure 10 has very little vertical material to support the load directly below the loading pin in the centre of the beam. This can be seen in Figure 16. As a result, the 5% beams failed a lot sooner than expected and at much lower metrics than the other three hexagonally infilled beams. The optimised beams significantly improve upon this by locating more material at the load points, which are the points of highest stress.

Figure 16: Photograph showing a 5% beam mounted on the Instron machine.

Optimised Beams This section focuses on the optimised beams. The reason the strength-to-weight ratios for the 3*Levels*, *Even*2 and *Even*3 optimised beams are higher than those for the hexagonally infilled beams is because the extra material has been added in the areas of the highest stress. The reason that the *Even*3 beam performed the best, compared to 3*Levels*, is because the amount of material which does not support much load, i.e. that in the top left and right corners, has been reduced by using a larger rectangular grid. The amount of supportive material used is similar to that in 3*Levels*, but the beam is lighter, which results in a better strength-to-weight ratio. Additionally, this larger grid is quicker to print as there are fewer lines for the printer to draw. This is the reason why *Even*3 has a strength-to-print-time ratio of 4.7 N/gram, which is higher than 3*Levels*, which has a score of 3.6 N/gram, which is similar to the

scores for the three heavier hexagonal beams. This shows that there is still a manual element to the strategy developed which can be used to modify some settings and thus provide additional improvements to component performance. These improvements show that the strategy developed in this research is successful in improving component performance compared to a current state of the art pattern (the hexagonal infill). The improvements also provides evidence to confirm that FEA results can be used to design an infill pattern.

The reason that the *Even*3 beam outperforms its predecessor *Even*2 is due to the addition of the third iteration, which adds the star pattern to the areas of highest stress. This is very effective because these areas are the areas which fail first, especially the section below the central loading pin at the top of the beam. Therefore strengthening these areas helps the beam support more load before it reaches yield point, without actually requiring the addition of much material. This confirms that the addition of the star pattern provides extra support and is beneficial. The 1*Level* beam was printed and tested to show the significant increase to the calculated metrics that adding the material in an optimised fashion to best support the load, as done in 3*Levels*, will have. The 1*Level* beam is just the regular rectangular grid, which is the predecessor of 3*Levels*, which has two more levels of iterations. The strength-to-weight ratio increased from 4.6 to 14.6 N/gram from 1*Level* to 3*Levels*, which is an increase of 217%. The strength-to-print-time ratio also increased from 1.7 to 3.6 N/minute which is an increase of 111%.

Failure Modes   The failure modes in which the beams failed during testing was also investigated. A difference in failure modes was noticed between the heavier and the lighter beams. Beams such as the 5% and the 10% beams experienced a long plastic region and at the end of loading they were still in tact, besides for a small crack underneath the central loading pin. Beams such as the 20% beam and *Even*3 experienced sudden brittle failure and cracked into two pieces after a shorter region of plastic deformation. A reason for this is that these heavier beams are much stiffer, especially the optimised beams, and thus resisted the deformation more until sudden brittle failure occurred. The cells directly below the central loading pin were always the cells to collapse first. A way to increase the strength of these cells would be to completely infill the cell. The MATLAB program developed allows for this, as additional threshold values and infill patterns can be used, such as the solid infill in cells.

7.2   Reliability of Results

All the beams tested were printed and tested three times to improve the reliability of the results. This was important because the print quality can vary from print to print. These variations can be as a result of different room temperatures due to sunlight reducing the speed at which the layers can cool. Every effort was made to ensure the print parameters were consistent, including the orientation, material, temperature and print settings. These have been discussed in Section 4.2. All the beams were loaded at a constant rate; 100 N/minute. If this loading rate was changed, to 200 N/minute for example, then it is possible that the results could vary from what was calculated, although this is unlikely to be significant.

The two machines available for testing the proof-of-concept beams and the hexagonally-infilled beams were the 1KN and the 25KN machines discussed in the Method 2 section. The resolution of these machines is as a function of their maximum load, measured in percent. The 20% beam and the 3*Levels* beam did not reach the yield point on the 1KN machine and so had to be reprinted and tested on the 25KN machine. A machine with a maximum load of 3KN would have been beneficial at it would have a higher resolution when compared to the 25KN machine as all of the test specimens failed before this 3KN point. The availability of a 3KN

machine would have improved the accuracy of the results. The advantages and disadvantages of the method used in this strategy have been discussed in the next section.

7.3 Advantages and Disadvantages of The Method

Advantages   The method used in this strategy, as described in Section 3, was chosen because it simplifies the 3D analysis into 2D cuts which were simpler to analyse and were easier to generate printable files for. The reason for this is that each 2D cut is independent of the next one so the optimisation for one 2D slice does not have to be used to optimise the next 2D slice. This would not be the case in Methods 1 and 2, where the entire model would need to be optimised at one time in 3D which would be computationally intensive and take longer to print.

The loading case of a rectangular-section beam under 3 point bending conditions was chosen as a proof of concept of the strategy developed in this research. The reason this case was chosen is because it is a well-known, widely applied and accepted standard test for evaluating the flexural strength of a component. It was simple to setup on the test machines and was simple to ensure the setup was the same for each beam being tested. Another advantage of the strategy developed is that the MATLAB programs have been designed to be easily modifiable by the user as all functions and variables have been defined parametrically. This means that the strategy can be used for any loading conditions for any beam or other structure and is thus a very adaptable and useful tool for designers. The method chosen is based on a regular rectangular grid which is very quick to print as it is made up of long straight lines which means the number of stops and starts is reduced as the printing is as continuous as possible. The MATLAB program also utilises various checks and optimisation to reduce the number of travel moves between print moves.

The strategy presented in this paper will result in exactly the same final topology if the same inputs are used. This makes it reliable and consistent. The strategy also uses additive iterations to optimise the infill pattern, which is better suited to the additive manufacturing process as mentioned earlier.

Disadvantages   The strategy developed in this research does also have some disadvantages. At present, the FEA mesh size will be the same size as the infill grid in the 3D print. The problem with this is that FEA is most accurate when the mesh size is very small. This is because there would be a greater number of elements, which means the elements are smaller and therefore the calculations made over each element are more accurate [34]. Furthermore, this strategy used first order cuboidal elements in the FEA mesh. Second order elements converge faster and would be more accurate than the first order elements used in this strategy [34]. However, with the current method, if the mesh size was made very small then the grid size would be so small that it would not be printable as there is a minimum spacing needed between each raster road which is printed. A better approach would be to have the infill mesh and the FEA mesh set to different sizes. This will allow the FEA model to have a very small mesh, resulting in a more accurate stress distribution but would still leave the infill mesh at a printable resolution. When calculating the stress in each cell in the infill mesh, the slicing software would have to take an average of the stress at every node in the equivalent area in the FEA stress distribution. This will result in more accurate infill optimisation. A further point is that the FEA model involves continuum elements but the final model created is a lattice structure. Some simplifications were needed to convert the continuum FEA stress distribution into one that could be discretised by a lattice structure in the form of the optimised infill pattern created.

In regards to the method of testing the proof-of-concept beams, the three point point bend test has disadvantages compared to a four point bend test. The results of the test are more sensitive to material imperfections in the specimen when compared to a four point bend test. This is because a four point bend test applies the load at two points which means that a much larger proportion of the beam reaches the maximum stress, as opposed to a three point bend test where only the section of the beam below the central loading pin is at maximum stress. This is problematic when testing brittle materials, as the higher central stress can initiate cracks and imperfections in the beam more so than the four point bend test.

The time taken to print the infills generated by this strategy could be decreased. The infill pattern would be kept the same but the commands generated for the 3D printer could be modified slightly. Currently, the program infills each cell individually, and goes through one by one until every cell which requires infilling has been filled in. This involves lots of small print moves and lots of travel moves. If longer print moves could be incorporated, then time savings could be made. A key area where long continuous print moves could be incorporated is when printing the cross-member patterns. As the diagonals all line up, a few long print moves could be used to infill lots of cells which all fall along a diagonal line.

The simply supported, centrally loaded, Michell framework was shown by Michell to be the most efficient possible in terms of strength per unit volume for that specific loading case [35]. A design very similar to this Michell framework could be used as the infill pattern for the rectangular section under 3 point bend conditions optimised earlier in this paper. This theoretical design would perform better than the optimised infill designed in this paper as it is has been shown to be the most efficient design as all the internal angles are $90\,^\circ$. However, even though this would be the optimum design in terms of strength per volume, which is synonymous to the strength-to-weight ratio used in this paper, it is an irregular, complex design to print and thus would not score as highly in the strength-to-print time metric. Additionally, the strategy developed in this paper can be used to optimise any structure with any loading conditions, whereas Michell's framework only works for one loading case and geometry.

The strategy developed in this paper is more concerned with the relative stress distribution across the component rather than the absolute stress values. Thus, if the magnitude of the loading conditions in the FEA were scaled down by a factor of 10, the same infill pattern would still be generated as the relative stress distribution across all of the nodes is the same. The optimised structure developed would need to be re-analysed in an FEA package to assess if the material it is designed from and its overall geometry is adequate to support the magnitude of the loading conditions. At present, the strategy only considers the direction and location of the loading.

7.4 Scope of Work

The subject of optimising infill patterns for 3D printed parts based on their loading conditions is a very new area of research as the topic is still in its infancy. The strategy developed in this research is applicable to any rectangular section beam and the programs designed in MATLAB are parametric and can be used to optimise a variety of structures based on their loading conditions. The proof of concept and testing performing in this research was limited to rectangular section beams under 3 point bending conditions.

There exists great potential to further develop this strategy. The MATLAB program created can be further developed to optimise the infill for any structure, as long as the exterior geometry can be created using Gcode by MATLAB the same way that the exterior rectangle is created in Gcode using the MATLAB program. There exist MATLAB functions that can load in *.stl* files

27

and if these were integrated into the strategy, then any shape or structure could be optimised. Integrating the FEA inside a graphical slicing package based on the strategy developed in this research would increase the usability of the optimisation process and allow it to expand into industrial use. Furthermore, if the FEA and optimisation were integrated into one package, then the optimised design could be re-analysed in the FE software to reiterate the design and ensure an optimum internal structure. Furthermore, another avenue which could be explored in terms of further work could modify the strategy developed in this paper and base the infill mesh on a hexagonal or a triangular grid. The cells which are higher stressed would still be infilled with more material. The next section will conclude the research presented in this paper.

8   Conclusion

3D printing has grown into a valuable tool for use by hobbyists at home and for use in manufacturing and rapid prototyping due to its short lead times and low waste. Slicing packages are used to convert 3D CAD models into a printable file. However, at present, slicing packages use standard infill patterns and infill percentages. There is no consideration of the components loading conditions when selecting the infill pattern or infill percentage. This results in non-optimised 3D printed parts.

The main aim of this research was to develop a strategy to optimise the infill pattern of 3D printed parts based on their loading conditions. The strategy splits the object up into a regular rectangular grid and then takes a stress distribution across the object, calculated in FEA, and puts more material in cells in the grid with a higher stress.

The proof of concept for this strategy was to consider a rectangular section beam under 3 point bending conditions. Optimised beams were designed using the strategy developed and were tested against hexagonally-infilled beams in a 3 point bend test. The yield point for all the samples was calculated and the strength-to-weight and strength-to-print-time metrics were calculated. The highest performing optimised beam achieved scores of 16.3 N/gram and 4.7 N/minute respectively compared to the highest performing hexagonally infilled beam which scored 10.5 N/gram and 3.7 N/minute respectively. The increase in performance of the optimised beam compared to the hexagonally infilled beam was 55% and 27% in the two metrics respectively. These increases in performance demonstrate the success of the strategy developed for improving the performance of the beams.

The strategy developed in this research has been set up parametrically so that it can be used to optimise any loading conditions for rectangular section beams. This has been shown in this paper where a cantilever beam loaded from its top face and one of its side faces was also optimised. The area of topology optimisation of 3D printed parts and infill is still in its infancy. Thus there exists great potential to further this work and develop algorithms to optimise shapes and structures more complex than rectangular-section beams.

9   References

[1] G. Hodgson. *Fused Filament Fabrication*. January 2014. Date Accessed: 30/03/2015. URL: `http://reprap.org/wiki/File:FFF.png#filelinks`.

[2] *UP Plus 3D Printer   Updated to the UP Plus 2*. January 2012. Date Accessed: 30/03/2015. URL: `http://3dprinting.co.nz/products/up-plus-3d-printer/`.

[3] *Slic3r Manual: Infill Patterns and Density*. January 2014. Date Accessed: 30/03/2015. URL: `http://manual.slic3r.org/expert-mode/infill`.

[4] J. Hornick and D. Rolland. *Many 3D Printing Patents Are Expiring Soon*. December 2013. Date Accessed: 16/04/2015. URL: `http://3dprintingindustry.com/2013/12/29/many-3d-printing-patents-expiring-soon-heres-round-overview/`.

[5] A. Palo. *3D printing market to grow to US16.2 billion in 2018*. March 2014. Date Accessed: 18/03/2015. URL: `http://www.canalys.com/newsroom/3d-printing-market-grow-us162-billion-2018`.

[6] C. Stamford. *Gartner Says Worldwide Shipments of 3D Printers to Reach More Than 217,000 in 2015*. October 2014. Date Accessed: 16/03/2015. URL: `http://www.gartner.com/newsroom/id/2887417`.

[7] L. Franceschi-Bicchierai. *Urbee 2 Is the 3D-Printed Car of the Future*. October 2013. Date Accessed: 10/03/2015. URL: `http://mashable.com/2013/03/01/urbee-3d-printed-car/`.

[8] R. Dhakshyani, Y. Nukman, A. Osman, and N. Azuan. FDM models and FEA in dysplastic hip. *Rapid Prototyping Journal*, 18:215 – 221, 2012.

[9] T. Hales. *The Honeycomb Conjecture*. May 2002.

[10] *Print Troubleshooting Pictorial Guide*. February 2015. Date Accessed: 25/03/2015. URL: `http://reprap.org/wiki/Print_Troubleshooting_Pictorial_Guide`.

[11] B. Huang and S. Singamneni. Raster angle mechanics in fused deposition modelling. *Journal of Composite Materials*, 49:363 – 383, 2015.

[12] B.M. Tymrak, M. Kreiger, and J.M. Pearce. Mechanical properties of components fabricated with open-source 3D printers under realistic environmental conditions. *Materials and Design*, 58:242 – 246, 2014.

[13] S.H Ahn, M. Montero, D. Odell, S. Roundy, and P.K. Wright. Anisotropic material properties of fused depostion modeling ABS. *Rapid Prototyping Journal*, 8(4):248 – 257, 2002.

[14] O. Luzanin, D. Movrin, and M. Plancak. Effect of layer thickness, deposition angle, and infill on maximum flexural force in FDM-built specimens. *Journal for Technology of Plasticity*, 39(1), 2014.

[15] B.H. Lee, M. Abdullah, and Z.A. Khan. Optimization of rapid prototyping parameters for production of flexible ABS object. *International Journal of Machine Tools and Manufacturing*, (169):54 – 61, 2005.

[16] V. Vijayaraghavan, A. Garg, J.S.L. Lam, B. Panda, and S.S. Mahapatra. Process charaterisation of.

[17] J.R. Hossain, D. Espalan, M. Perez, and R. Wicker. Improving tensile mechanical properties of FDM-manufacutred specimens via modifying build parameters. 2013.

[18] N. Umetani and R. Schmidt. Cross-sectional structural analysis for 3D printing optimisation. 2013.

[19] U. Schramm and M. Zhou. Recent developments in the commercial implementation of topology optimisation.

[20] M. Zhou, R. Fleury, Y.K. Shyy, H. Thomas, and J.M. Brennan. Progress in topology optimization with manufacturing constraints. *Altair Engineering, Inc.*

[21] M. Tomlin and J. Meyer. Topology optimization of an additive layer manufactured.

[22] I. Brackett, I. Ashcroft, and R. Hague. Topology optimization for additive manufacturing. *Loughborough University*, 2011.

[23] L. Lu, A. Sharf, H. Zhao, Y. Wei, Q. Fan, X. Chen, Y. Savoye, C. Tu, D. Cohen-Or, and B. Chen. Build-to-last: Strength to weight 3D printed objects. *ACM Trans. Graph.*, 33(4):97:1–97:10, 2014.

[24] *Simplify3D Software*. 2014. Date Accessed: 15/04/2015. URL: `https://www.simplify3d.com/software/m`.

[25] M. Troy. *Altair OptiStruct Revolutionizes Lattice Structures for 3D Printing*. Feb 2015. Date Accessed: 15/04/2015. URL: `http://www.altair.com/(X(1)S(uihmrlgoujmnnlxjre0xmzna))/NewsDetail.aspx?news_id=11109&Aspx`.

[26] J. Van der Geest. *INSERTROWS (v2.0, may 2008)*. May 2008. Date Accessed: 30/03/2015. URL: `http://uk.mathworks.com/matlabcentral/fileexchange/9984-insertrows--v2-0--may-2008-/content/insertrows.m`.

[27] H. Thomas. *Anisotropic material properties of fused depostion modeling ABS*. 2014.

[28] *2519-100 Series Load Cells*. 2003. Date Accessed: 31/03/2015. URL: `http://www.artisantg.com/info/PDF__496E7374726F6E5F323531395F3130305F4461746173686565742.pdf`.

[29] *Instron 3343 1 kN Single Column Testing Systems*. 2003. Date Accessed: 31/03/2015. URL: `http://vecomtech.com/en/single-column-utm/instron-3343-1-kn-single-column-testing-systems.html`.

[30] *Filament volume and length*. July 2013. Date Accessed: 25/03/2015. URL: `http://www.toybuilderlabs.com/blogs/news/13053117-filament-volume-and-length`.

[31] R. Hagen. *Basics of PLA*. July 2013. Date Accessed: 26/03/2015. URL: `http://www.uhde-inventa-fischer.com/linkservid/14D9B34D-5056-A765-BB1E731580EA135C/showMeta/0/`.

[32] H.A Eschenauer and N. Olhoff. Topology optimization of continuum structures:a review. *Applied Mechanics Review*, 54(4):331 – 390, 2001.

[33] S.C. Burgess. *Shape factors and material indices for dimensioally constrained structures - Part 1: beams*, volume 214. 1999.

[34] P. Dvorak. *Avoiding pitfalls in FEA*. October 2013.

[35] S.C. Burgess. *The Ranking of efficiency of structural layouts using form factors - Part 2: design for strength*, volume 212. 1997.

10 Appendices
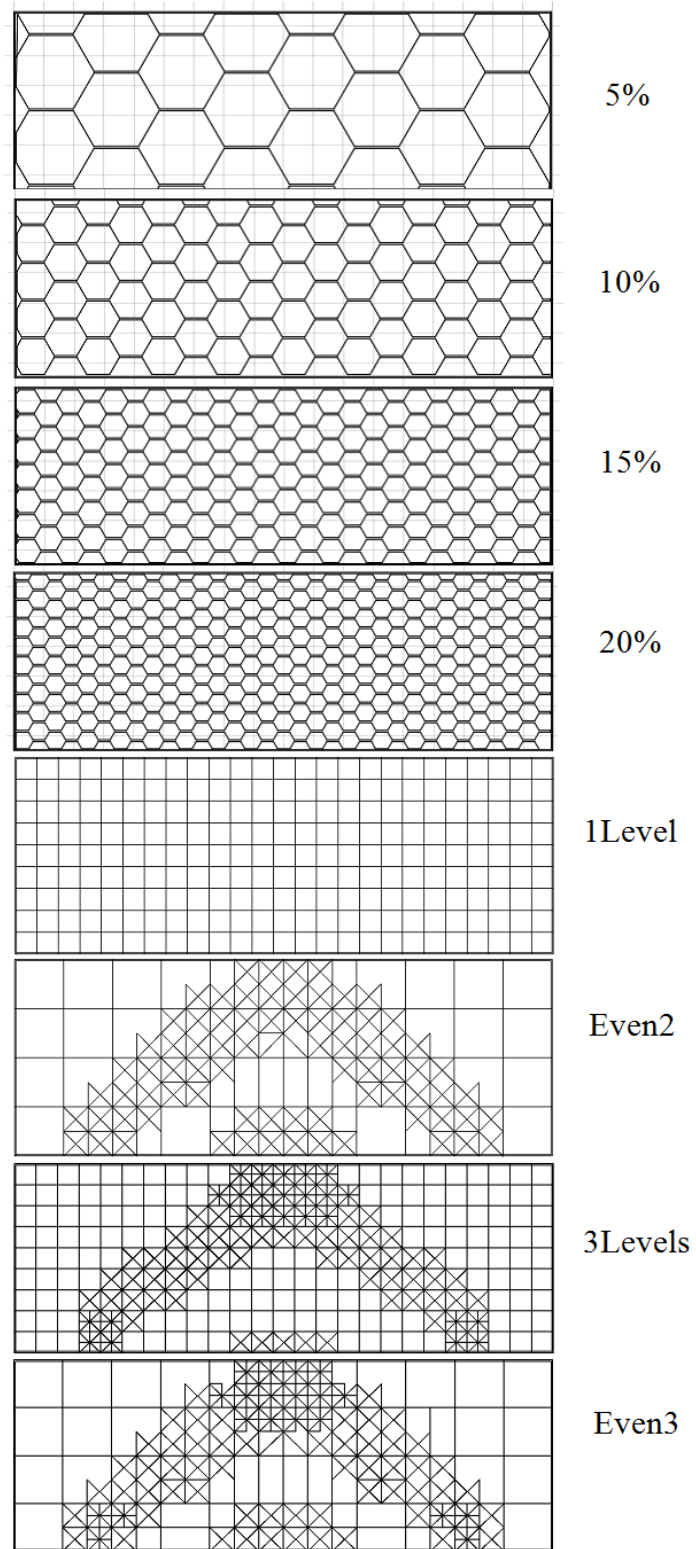
10.1 Appendix 1 - Beams Tested

Figure 17: Renders of all the beams printed and tested.

10.2 Appendix 2 - Table of Results

		Print Time	Weight (grams)	Yield Point (N)	Strength/weight (N/gram)	Strength/Print Time (N/minute)
5%	1	56	28.54	75	2.6	1.3
	2	56	27.32	90	3.3	1.6
	3	56	28.34	80	2.8	1.4
	Mean	**56**	**28.07**	**82**	**2.9**	**1.5**
10%	1	1h40	42.77	348	8.1	3.5
	2	1h40	43.38	415	9.6	4.2
	3	1h40	43.74	316	7.2	3.2
	Mean	**1h40**	**43.30**	**360**	**8.3**	**3.6**
15%	1	2h29	57.45	600	10.4	3.8
	2	2h29	57.36	500	8.7	3.1
	3	2h29	57.49	550	9.6	3.5
	Mean	**2h29**	**57.43**	**550**	**9.6**	**3.5**
20%	1	3h27	74.24	760	10.2	3.7
	2	3h27	74.1	770	10.4	3.7
	3	3h27	72.03	790	11.0	3.8
	Mean	**3h27**	**73.46**	**773**	**10.5**	**3.7**
1levelgrid	1	1h47	38.97	176	4.5	1.6
	2	1h47	38.64	182	4.7	1.7
	3	1h47	38.64	178	4.6	1.7
	Mean	**1h47**	**38.75**	**179**	**4.6**	**1.7**
3levels	1	3h55	57.17	900	15.7	3.8
	2	3h55	57.18	900	15.7	3.8
	3	3h55	57.04	708	12.4	3.0
	Mean	**3h55**	**57.13**	**836**	**14.6**	**3.6**
Even 2	1	2h48	45.51	700	15.4	4.2
	2	2h48	45.24	620	13.7	3.7
	3	2h48	44.5	628	14.1	3.7
	Mean	**2h48**	**45.08**	**649**	**14.4**	**3.9**
Even 3	1	3h21	49.21	780	15.9	3.9
	2	3h21	49.53	900	18.2	4.5
	3	3h21	49.34	736	14.9	3.7
	Mean	**3h21**	**49.36**	**805**	**16.3**	**4.0**

Table 2: Results table from the testing.

10.3   Appendix 3 - Force-Extension Graphs
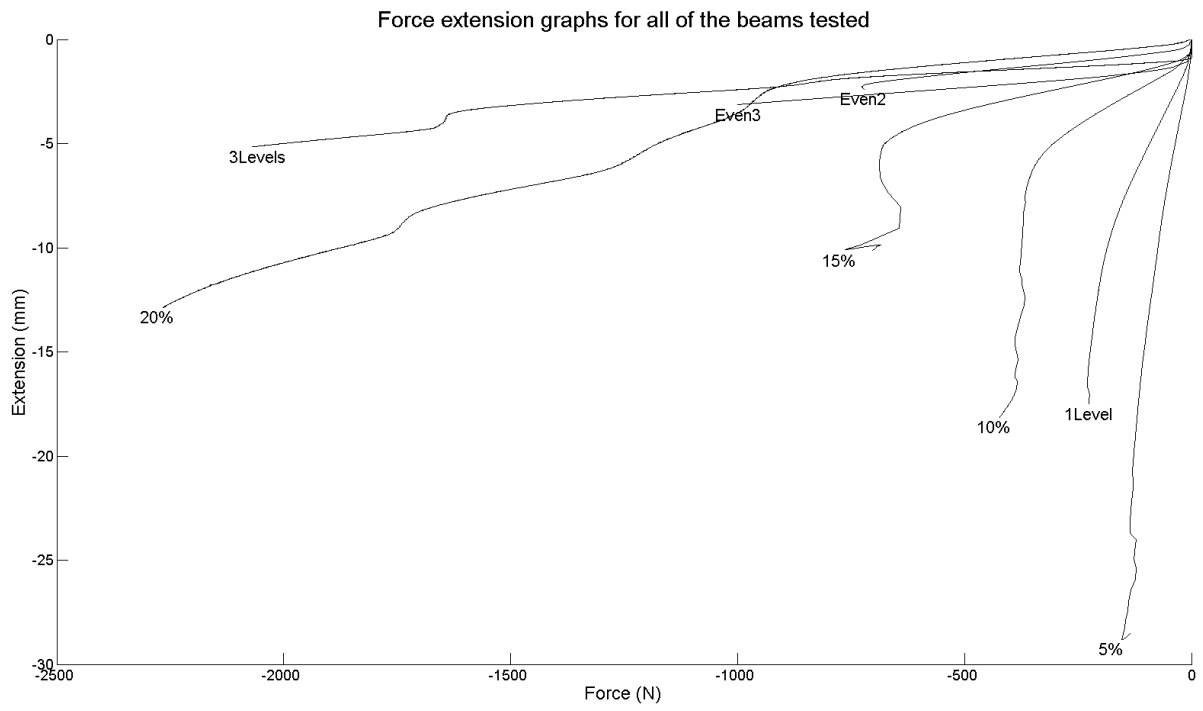
Force extension graphs for all of the beams tested

Figure 18: Force-extension graphs for all of the beams tested.